International Journal of Architectural, Civil and Construction Sciences
ISSN: 2415-1734
Vol:13, No:2, 2019

Experimental and Numerical Study of Ultra-High-Performance Fiber-Reinforced Concrete Column Subjected to Axial and Eccentric Loads

Chengfeng Fang, Mohamed Ali Sadakkathulla, Abdul Sheikh

***Abstract*—**Ultra-high-performance fiber reinforced concrete (UHPFRC) is a specially formulated cement-based composite characterized with an ultra-high compressive strength ($f_c^{'}$ = 240 MPa) and a low water-cement ratio (W/B= 0.2). With such material characteristics, UHPFRC is favored for the design and constructions of structures required high structural performance and slender geometries. Unlike conventional concrete, the structural performance of members manufactured with UHPFRC has not yet been fully studied, particularly, for UHPFRC columns with high slenderness. In this study, the behaviors of slender UHPFRC columns under concentric or eccentric load will be investigated both experimentally and numerically. Four slender UHPFRC columns were tested under eccentric loads with eccentricities, of 0 mm, 35 mm, 50 mm, and 85 mm, respectively, and one UHPFRC beam was tested under four-point bending. Finite element (FE) analysis was conducted with concrete damage plasticity (CDP) modulus to simulating the load-middle height or middle span deflection relationships and damage patterns of all UHPFRC members. Simulated results were compared against the experimental results and observation to gain the confidence of FE model, and this model was further extended to conduct parametric studies, which aim to investigate the effects of slenderness regarding failure modes and load-moment interaction relationships. Experimental results showed that the load bearing capacities of the slender columns reduced with an increase in eccentricity. Comparisons between load-middle height and middle span deflection relationships as well as damage patterns of all UHPFRC members obtained both experimentally and numerically demonstrated high accuracy of the FE simulations. Based on the available FE model, the following parametric study indicated that a further increase in the slenderness of column resulted in significant decreases in the load-bearing capacities, ductility index, and flexural bending capacities.

***Keywords*—**Eccentric loads, ductility index, RC column, slenderness, UHPFRC.

I. Introduction

NOWADAYS, more and more high-performance base designs are demanded to accommodate the highly developed human civilizations over the world. UHPFRC is a promising construction material featured with superior mechanical strength, exceptional self-consolidating characteristics, and high corrosion resistance, making it attractive to cater the demand of high-performance base designs. To date, most of current researches are focusing on studying optimizations of the UHPFRC mix [1], [2], flexural behaviors of UHPFRC beams or slabs [3]-[6], and structural response of UHPFRC structural members under blast loads [7]. As demonstrated from these studies, structural members manufactured with UHPFRC exhibited an improved structural performance compared to companion members made with normal strength concrete (NSC), which hence highlights the enormous potential and importance of UHPFRC in the future applications. Owing to its high compressive concrete strength, UHPFRC is particularly favorable for the designs and constructions of highly loaded columns compared to NSC or composite materials [8]. Experimental studies investigating pure axial behaviors of short columns were conducted by Shin et al [9]-[11] and Hosinieh et al. [12]. These studies indicated that reductions in spacing of transverse reinforcements of the short column resulted in significant improvements in load bearing capacities and load sustainability after peak. Furthermore, with the constant stirrup spacing, providing additional crosstie for the transverse reinforcements would only enhance the total toughness of the short columns without significant improvements in their load bearing capacities. Meanwhile, an effective control in concrete spalling at failure was benefited by the presence of steel fibers, and it subsequently improves the post-peak ductility of the columns. To fully understand the behaviors of RC columns in structures, structural performances of UHPFRC columns subjected to both axial compression and flexural bending moment were experimentally investigated by Steven and Empelmann [13] and Hung et al [14]. Relationships of load to moment interactions and force to axial deformation were extracted to assess the influence of eccentricity and slenderness regarding the load bearing capacities and ductility index of the columns.

Replacing conventional concrete by the UHPFRC to achieve high-performance base designs allows the column member to have a reduced member cross-section and a significantly higher load bearing capacity. Conversely, the subsequent effects of the increased slenderness induced by the reduced member cross-section in regards to the structural performance of the UHPFRC column have not been fully studied. Hence, in order to address this shortcoming, an experimental study was conducted for exploring the structure performance of slender UHPFRC columns under concentric or eccentric load. Subsequent FE analysis was conducted by using the software package ABAQUS to simulate the load-middle height or middle span deflection relationships as well as corresponding damage patterns for all UHPFRC members. Further

Chengfeng Fang is Ph.D. student, Mohamed Ali Sadakkathulla is Senior Lecturer, and Abdul Sheikh is Associate professor in the School of Civil, Environmental and Mining Engineering (CEME) at University of Adelaide, Adelaide, Australia (e-mail: chengfeng.fang@adelaide.edu.au, mmsadakk@civeng.adelaide.edu.au, abdul.sheikh@adelaide.edu.au).

clarification was conducted by comparing the simulated results against the experimental results for pursuing parametric studies associated with the effects of slenderness.

II. Experimental Program

The experimental program consists of two main stages of testing, including material tests and structure tests. Material tests were conducted to characterize stress-strain responses of UHPFRC under compression or tension, and another objective for material tests is to clarify existing confinement model by comparing the stress-strain response obtained analytically against the stress-strain response measured from the tests. The primary objectives for structure testing are listed as follows:

1. To generate load-axial strain and load mid-height deflection responses for slender UHPFRC columns in order to provide insight into the effects of eccentricities regarding the structural performance of the columns.
2. By conducting a four-point flexural bending test on UHPFRC beam with an identical reinforcement arrangement as tested columns, a complete load-moment interaction envelope was generated to provide some guidelines with the design of slender UHPFRC columns.

A. UHPFRC Mix and Preparation

The ingredients used for manufacture of UHPFRC mix were shown in Table I. To be noted that the river washed sand and silica fume (*EcoTech*) were particularly sourced with average size of 400 μm and 50 μm, respectively, to ensure the fineness and high homogeneity of the concrete mix. Additional hook end steel fibers (2.25% by volume) with a diameter of 0.55 mm and a fiber length of 35 mm featured with a tensile strength of 1345 MPa were added in the mix to attain a ductile tensile behavior of the UHPFRC. Complying with AS1012, the dry constituents as described above were pre-calculated and electronically weighted. All dry ingredients were mixed in the concrete mixer for approximately 5 minutes, after which the water and superplasticiser were added into the mix. Subsequently, hook-end steel fibers can be added whenever the concrete mix attend a good flowability, and further 5 minutes of mixing were required for allowing steel fiber evenly distributed in the concrete mix.

B. Material Tests for Properties Characterization:

Unconfined cylinders with a diameter of 100 mm and a height of 200 mm were casted in accordance with AS 1012, and tested under uniaxial compression with a loading rate of 0.05 mm/minutes for the determination of compressive stress-strain response, as shown in Fig. 1 (a). Direct tensile tests were conducted on unnotched dog-bone specimens as recommended by Wille et al. [15] to obtain the axial tensile stress-strain relationship as well as strain hardening behavior of UHPFRC, as presented in Fig. 1 (b). By performing these tests, the compressive and tensile strengths of UHPFRC have been characterized as 145.4 MPa and 5.8 MPa, respectively, and Young's modulus of UHPFRC was determined as 44 GPa. Overall, these material properties were required as fundamental input to process following numerical analysis.

TABLE I
Mixture Proportion

Components	Note	Mass/Cement Ratio
Cement	Sulphate resistant	1
River washed sand	Average size of 400 μm	1
Silica Fume (*EcoTech*)	Average size of 50 μm	0.266
Steel fibre (V_f=2.25%)	Hook-end fibres	0.175
Water	-	0.17
Superplasticiser (*Visconcrete 10*)	Water reducing admixture	0.565

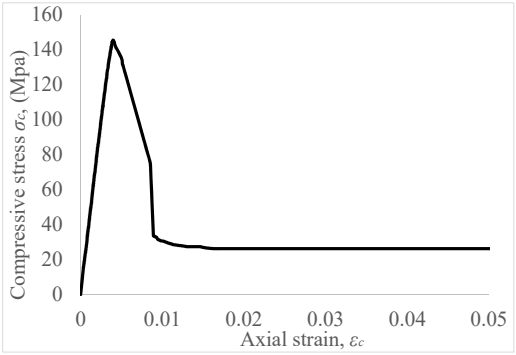

(a)

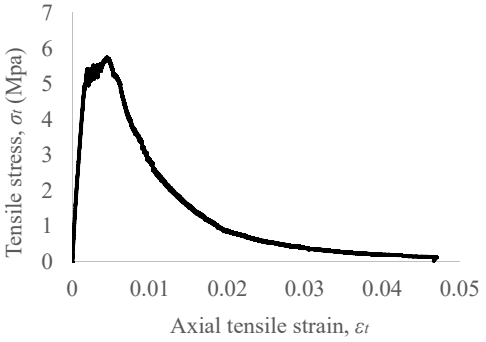

(b)

Fig. 1 Material properties of (a) compressive stress-strain response for unconfined and confined UHPFRC (b) tensile characterizations of UHPFRC

C. Test Specimens and Test Setup

As presented in Fig. 2 (a), all UHPFRC members have a square cross-section with a width of 150 mm and reinforced by four longitudinal reinforcements with a diameter of 16 mm. Transverse reinforcements with a width of 110 mm were casted in the UHPFRC, allowing a concrete cover of 20 mm and a stirrup spacing of 85 mm as shown in Fig. 2. Four slender UHPFRC columns with a length of 1600 mm were tested in the Amsler machine with uniaxial loading at eccentricities of 0, 35, 50, and 85 mm, as presented in Fig. 2 (b). A load-controlled loading rate for all tested column is 50 kM/minute. Moreover, one UHPFRC beam with a span of 2850 mm was tested under four-point bending using a 1000 kN capacity Avery machine, as shown in Fig. 2 (c). Instrumentations and test setups can be observed in Fig. 2, where the boundary conditions for the top and bottom of the columns were both pins that allow rotating at

the edges of the column. To measure the axial deformation of the columns during loading, LVDT 1-4 with a gauge length of 800 mm were placed vertically at the centerline of each column face, as presented in Figs. 2 and 3. Furthermore, three LVDTs were placed horizontally pointing at the compressive face of the column with a constant space of 300 mm for recording the lateral deflections of the columns. Stain gauges were placed on the middle height of the columns surface and longitudinal reinforcements to record corresponding strains. Similarly, LVDTs 1-3 with a gauge length of 200 mm were placed at the bottom of the beam to measure the displacements at the middle span, and the average mid-displacement was determined and the corresponding moment at failure was found by analyzing the bending moment diagram for the structure. LVDTs 4-7 with a gauge length of 500 mm were placed at two sides of the beam for measuring the rotations of the beam during the static loading that was applied on the top of the beam, as shown in Figs. 2 and 3.

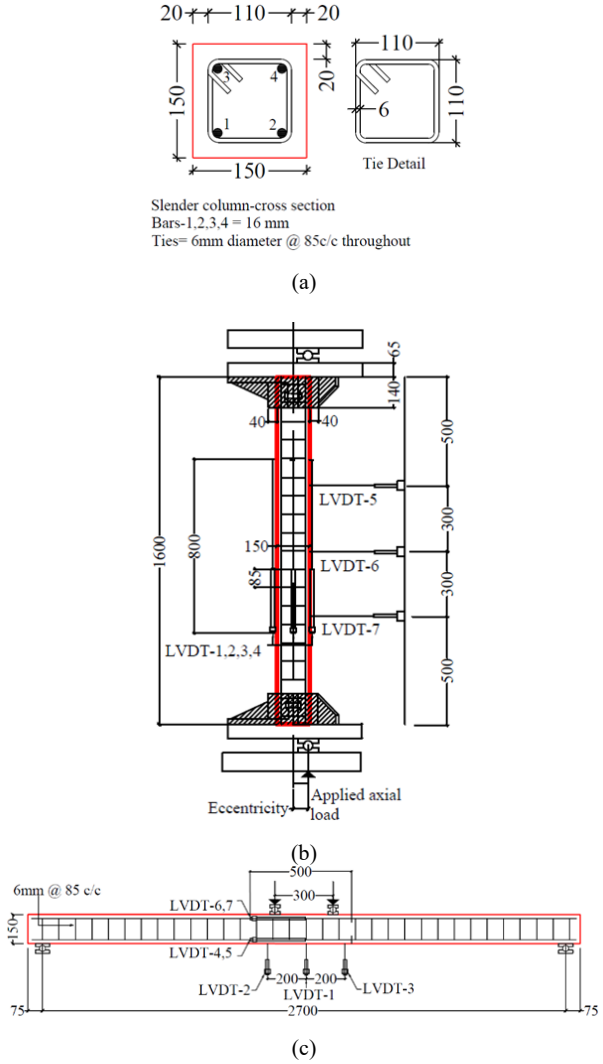

Fig. 2 Test specimen details and instrumentation set up: (a) cross-section of the beam and columns; (b) concentrically and eccentrically loaded columns; (c) four point-bending tests for the beam

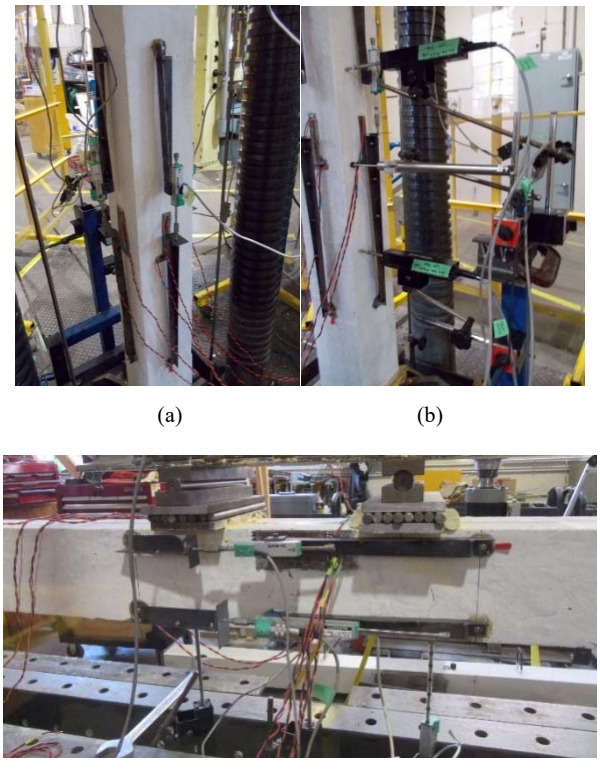

(a) (b)

(c)

Fig. 3 LVDT setup for UHPFRC members (a) longitudinal LVDTs measuring axial deformations of slender columns (b) horizontal LVDTs measuring lateral deformations of slender columns (c) longitudinal and vertical LVDTs measuring rotations and vertical deformations of UHPFRC beam

III. Experimental Results

A. Cracking Pattern and Failure Mode

The failure of the concentrically loaded column was violet with a large area of concrete spalling occurred at the top of the column, as presented in Fig. 4 (a). The corresponding strain recorded by the strain gauge placed at the middle height of the column is 0.00369, which is slightly lower than the crushing strain of 0.004 identified from the cylinder compression tests. This suggested that the concrete spalling failure for concentrically loaded column normally occur at the top and bottom regions instead of middle height region, and this phenomenon mainly attributed to the high stress concentration appealed at the top and bottom of the column.

A typical failure mode for eccentrically loaded column was represented in Fig. 4 (b). Concrete spalling was observed at the compression face of the column due to concrete softening, and a flexural tensile crack induced by excessive bending moment was appealed at the tensile face of the column. Hence, a plastic hinge was formed at the middle height of the slender UHPFRC column, and the lateral deflection was enlarged with a further increase in the rotation of the hinge. For UHPFRC beam shown in Fig.4 (c), it is apparent that the member was failed due to two

flexural tensile cracks caused by insufficient bending capacity.

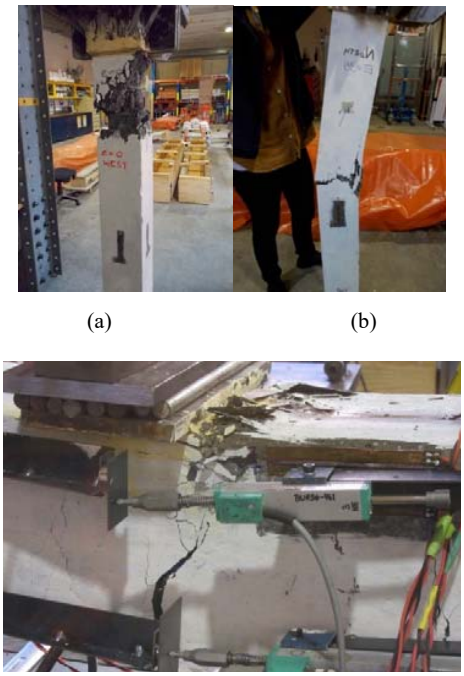

(a) (b)

(c)

Fig. 4 Failure modes of (a) concentrically loaded column (b) eccentrically loaded column (c) beam under four-point bending

B. Load-Axial Strain Relationship and Load Bearing Capacity

Test results are summarized in Table II, and load-axial strain relationships of columns are presented in Fig. 5. Comparisons in load bearing capacities (P_u) of columns indicate that the values of P_u decrease dramatically with an increase in eccentricity of axial load, particularly, more than 60% of reduction in P_u was observed. By considering the secondary moment effect caused by the lateral deflection ($\delta_{mid\text{-}peak}$) at the peak load, the flexural bending capacities (M_u) were estimated and shown in Table II. Column SL-50 has the highest M_u compared to companion specimens, whereas the M_u of column SL-35 is slightly lower than that of column SL-50. Based on this, it can be deducted that the balance condition for eccentrically loaded columns might occurred when the eccentricity range from 35 mm to 50 mm. Strains in concrete (ε_{conc}) measured from the middle height of the columns reveal that the concrete softening was occurred at the middle height of all eccentrically loaded columns. The ductility index (I_{10}) was used to evaluate deformability and energy absorption capacity of the columns, and hence to assess the structural performance of the column in application. Detail definitions regarding the ductility index (I_{10}) can be referred to Foster and Attard [16]. Based on the definition, it gives that I_{10} = 1 for describing a perfectly elastic-brittle material and I_{10} = 10 for describing a perfectly elastic-plastic material, and hence a large value of I_{10} represents a considerable good ductility of the column. Comparisons in I_{10} among the slender UHPFRC columns demonstrate that column SL-35 has the highest ductility compared to companion columns. While for columns SL-50 and SL-85, the values of I_{10} remain around 7.7-7.9, indicating that the ductility of eccentrically loaded columns was not influenced by further increment in eccentricity after the balance condition of the column.

TABLE II
TEST RESULTS OF ALL COLUMNS AND BEAM

Specimen	P_u (kN)	M_u (kN.m)	$\delta_{mid\text{-}peak}$ (mm)	$\delta_{mid\text{-}ult}$ (mm)	ε_{conc}	I_{10}
SL-0	3199.3	1.2	0.4	29.8	0.00369	4.6
SL-35	1233.9	61.2	14.6	73.9	0.00413	9.3
SL-50	910.2	64.1	20.5	74.1	0.00406	7.7
SL-85	480.5	53.6	26.6	61.7	0.00404	7.9
SL-beam	-	32.8	76.7	129.3	0.00401	-

The mid-height deflections at the peak load along the length of columns were exhibited in Fig. 6. It is worth mentioning that increase in eccentricities facilitate the lateral deflection at the middle-height of the columns, which can be explained by the fact that severe buckling was occurred at the middle height of the columns (SL-35, SL-50, SL-85) with an increase in eccentricity.

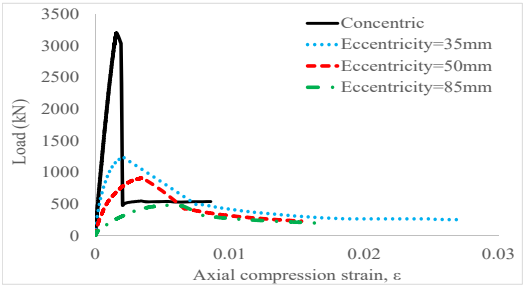

Fig. 5 Load versus axial compression strain of slender columns

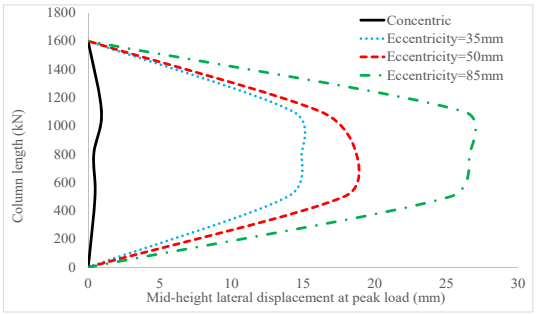

Fig. 6 Column length versus mid-height lateral deflection at peak load of slender columns

IV. FE ANALYSIS

FE analysis was conducted to simulate the structure response of slender UHPFRC columns under concentric and eccentric loading conditions. Clarifications of FE models were conducted to compare simulated load-middle height deflection responses against experimental results, and a further parametric study regarding slenderness of column can be undertaken.

A. FE Modelling

As presented in Fig. 7 (a), concrete geometry was modelled with 3D hexahedral solid elements featured with eight nodes (C3D8R), and steel reinforcements were identified as truss elements in 3D space featured with two nodes (T3D2). To be specifically, unconfined and confined concrete elements were defined separately, where confined UHPFRC was modelled as a solid element surrounded by a square hollow section identified as unconfined UHPFRC. A tie constrain was adopted to define a perfect bonding for the interface between unconfined and confined UHPFRC, and integrated geometry of unconfined and confined UHPFRC was defined as an embedded region for the steel reinforcements (truss elements). To simulate the experimental setup, steel caps composited with a rectangular flat plate (length: 500 mm, breadth: 350 mm, thickness: 65 mm) and a square ring (length: 165 mm, thickness: 45 mm) were identified as 3D elements (C3D8R) with an elasto-plastic behavior assigned, as presented in Fig. 7 (b). By defining a reference point with a multiple point coupling constrains assigned on the steel caps, the slender UHPFRC columns were loaded concentrically and eccentrically with a steady rate (0.15 mm/min).

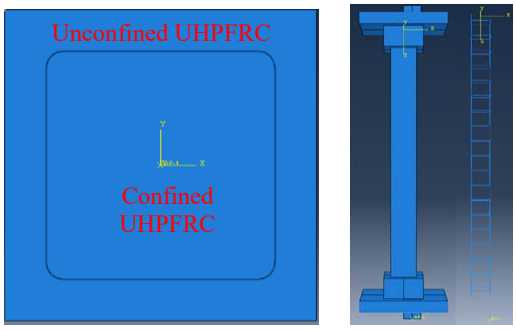

(a) (b)

Fig. 7 FE modelling of (a) Cross-section of UHPFRC slender columns (b) UHPFRC slender column and reinforcement

In this study, a CDP model in ABAQUS was adopted to perform the elastic-plastic material properties of UHPFRC. With parameters of plasticity and elasto-plastic responses of UHPFRC under tension and compression defined in the model, the structural performance of slender UHPFRC columns under concentric or eccentric loads was able to be accurately simulated.

B. Comparisons of Experimental and Simulated Results

Fig. 8 shows well correlations between experimental results and FE simulation, which further highlights the applicability and accuracy of the proposed FE models for predicting the load-middle height deflection relationships of UHPFRC columns. Meanwhile, the concrete damage patterns of the UHPFRC columns under compression were simulated by using the CDP model in conjunction with the definition of damage parameters. As presented in Fig. 9 (a), the concrete spalling at the compressive face of the column SL-50 was appropriately simulated in the FE model, where a maximum compressive damage level of 86% was represented at the middle-height of the column. Additionally, a single flexural crack occurred at the middle-height of the column SL-50, as presented in Fig. 9 (b), was well captured by the FE model with a maximum tensile damage of 98% observed. Similarly, concrete damage patterns for other columns were simulated and compared against the experimental observations; consequently, high agreements in load-middle height deflection responses and concrete damage patterns further highlight the reliability of the proposed FE models.

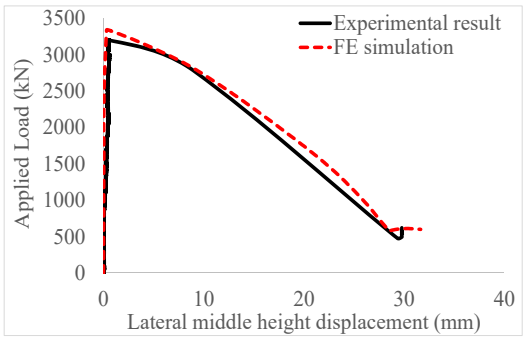

(a)

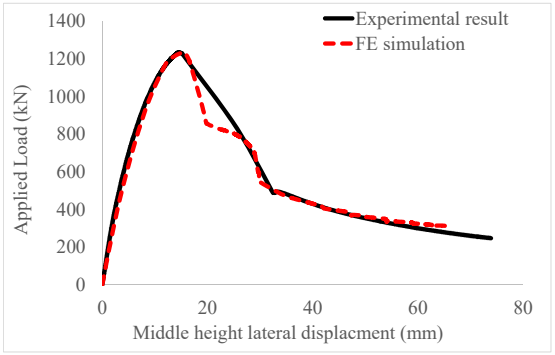

(b)

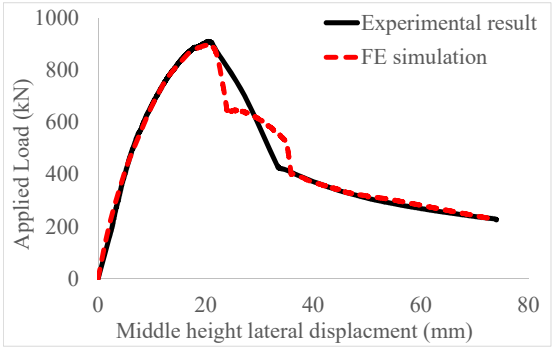

(c)

Fig. 8 Comparisons among experimental results and FE simulation for UHPFRC members (a) concentrate (b) eccentricity = 35 mm (c) eccentricity = 50 mm

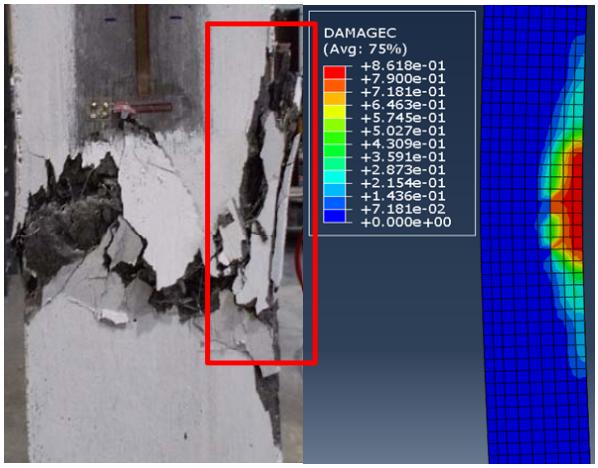

(a)

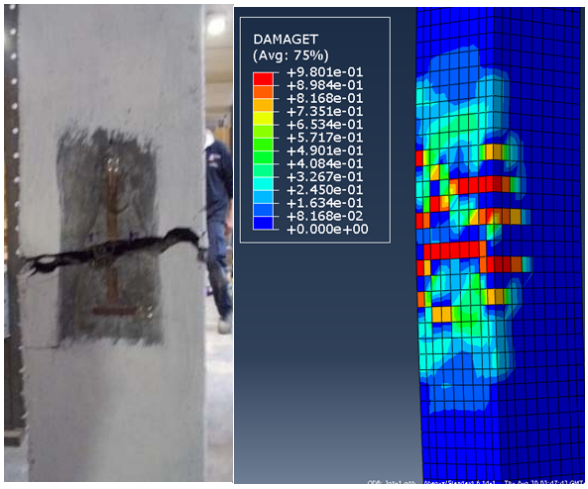

(b)

Fig. 9 Comparisons between failure mode and compressive FE cracking pattern for the column loaded with eccentricity of 50mm (a) compressive damage pattern (b) tensile damage pattern

C. Comparisons of Load-Moment Interaction Curves

A complete load-moment (P-M) interaction envelope was obtained by integrating experimental results for slender UHPFRC columns loaded with eccentricities from 0 mm to 85 mm, as shown in Fig. 10. It is worth mentioning that comparisons between envelopes obtained experimentally and numerically exhibited a considerably good agreement between the curves, and even for the loading lines developed from FE model closely match with the loading lines obtained numerically. For slender UHPFRC column loaded concentrically, FE model slightly overestimates the load bearing capacity of the column, and this might due to the unexpected fiber confinement effects or fiber edge effects.

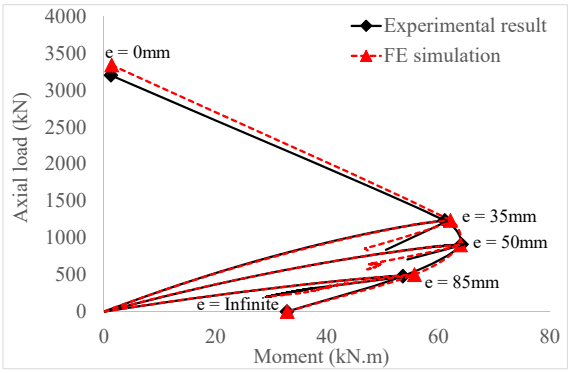

Fig. 10 Load-Moment interaction diagram for UHPFRC slender columns

V. Parametric Study for Slenderness Effect

TABLE III
Effects of Slenderness Ratio (λ) Pertaining to Load-Moment Interaction Relationships

e (mm)	P_u (kN)				M_u (kN.m)			
	37	57	67	77	37	57	67	77
0	3199.3	3319	3287	1746	1.2	0.8	0.6	3.1
35	1233.9	832	662	532	61.2	56.1	51.5	42.4
50	910.2	619	509	421	64.1	55.9	51.4	46.7
85	480.5	368	321	278	53.6	49.9	47.5	45.5

With this confidence, an extended parametric study was conducted numerically through FE modelling. With an identical cross-section and the same steel reinforcement arrangement, the effects of slenderness of column regarding the load bearing capacity and moment capacity were investigated by differing the length of UHPFRC columns. To achieve this, newly defined lengths of the UHPFRC columns were 2450 mm, 2875 mm, and 3300 mm. According to the AS3600, the slenderness ratio (λ) can be calculated in (1) and (2).

$$\lambda_n = \frac{kl_u}{r_g} \tag{1}$$

$$r_g = \sqrt{\frac{I}{A}} \tag{2}$$

where, k is defined as an effective length factor to reflect the boundary and lateral bracing conditions of the column (for pin to pin condition, k=1); l_u is unsupported column length; r_g is the radius of gyration, defined in (2). According to AS3600, the slenderness ratio (λ) for the tested column was initially 37, and the slenderness ratios for the newly defined columns were 57, 67, and 77, respectively. Tested results and simulated results for parametric studies were summarized in Table III. Comparisons in Table III indicated that an increase in slenderness ratio (from 67 to 77) resulted in a significant reduction (nearly 50%) in the load bearing capacity of the concentrically loaded column, and this mainly due to the buckling occurred at the middle height of the column, which

severely compromised its load bearing capacity. For eccentrically loaded column, increases in slenderness led to decreases in both load bearing and bending moment capacities, as presented in Table III. Specifically, an increase in slenderness ratio (λ) from 37 to 77 resulted in a reduction (57%) in load bearing capacity of the column loaded with eccentricity of 35 mm. Meanwhile, the increase in slenderness ratio also resulted in a reduction of 31% in the moment bending capacity. Whilst for slender columns loaded with eccentricity of 85mm, an increase in slenderness ratio (λ) from 37 to 77 led to a reduction of 42% in load bearing capacity and a reduction of 15%, respectively. Hence, this indicated that slender UHPFRC columns under large eccentricities, the decreases in both load bearing capacity and bending moment capacity due to increasing slenderness ratio were less significant compared to the columns loaded with small eccentricity.

VI. Conclusion

In order to study the behaviors of slender UHPFRC columns, four UHPFRC columns with varying eccentricity of loading were tested under concentric and eccentric loads. The major findings of this paper are summarized as follows:

1) With the flexural bending introduced by the eccentricity, the load bearing capacity of eccentrically loaded column was severe compromised.
2) Experimental results indicated that the balance condition featured with the maximum bending capacity for eccentrically loaded columns might occur when the eccentricity ranges from 35 mm to 50 mm. The ductility index of eccentrically loaded column has no significant influence by increment in eccentricity after the balance condition of the column.
3) With the assistance of the FE models, the slenderness effects pertaining to load bearing and bending moment capacities were studied: slenderness ratio = 77 could be a threshold that might result in a huge compromise in load bearing capacity of the concentrically loaded UHPFRC columns in practice.
4) To increase slenderness ratio (λ) in the design of UHPFRC column, it would result in a considerably large compromise in both load bearing capacity and bending moment capacity for the slender columns loaded with small eccentricities.

References

[1] T. Xie, C. Fang, M. S. Mohamad Ali, and P. Visintin, "Characterizations of autogenous and drying shrinkage of ultra-high performance concrete (UHPC): An experimental study," *Cement and Concrete Composites*, vol. 91, pp. 156–173, 2018.
[2] D. Y. Yoo, N. Banthia, Y. S. Yoon, "Effectiveness of shrinkage-reducing admixture in reducing autogenous shrinkage stress of ultra-high-performance fiber-reinforced concrete," *Cement and Concrete Composites*, vol. 64, pp. 27–36, 2015.
[3] F. Baby, P. Marchand, M. Atrach, F. Toutlemonde, "Analysis of flexure-shear behavior of UHPFRC beams based on stress field approach," *Engineering Structures*, vol. 56, pp. 194–206, 2013.
[4] G. H. Mahmud, Z. Yang, A. M.T. Hassan, "Experimental and numerical studies of size effects of Ultra High Performance Steel Fibre Reinforced Concrete (UHPFRC) beams," *Construction and Building Materials*, vol. 48, pp. 1027–1034, 2013
[5] F. Baby, P. Marchand, F. Toutlemonde, "Shear Behavior of Ultrahigh Performance Fiber-Reinforced Concrete Beams. I: Experimental Investigation," *Journal of Structural Engineering*, vol. 140, no. 5, 2014.
[6] F. Lachance, J. P. Charron, and B. Massicotte, "Development of Precast Bridge Slabs in High-Performance Fiber-Reinforced Concrete and Ultra-High-Performance Fiber-Reinforced Concrete," *ACI Structural Journal*, pp. 929–939, 2016.
[7] S. G. Millard, T. C. K. Molyneaux, S.J. Barnett, and X. Gao, "Dynamic enhancement of blast-resistant ultra high performance fibre-reinforced concrete under flexural and shear loading," *International Journal of Impact Engineering*, vol. 37, pp. 405-413, 2010.
[8] M. Empelmann, M. Teautsch, and G. Steven, "Expanding the application range of RC-columns by the use of UHPC", *Tailor Made Concrete Structures*, pp. 461-468, 2008.
[9] H. O. Shin, Y. S. Yoon, S. H. Lee, W. D. Cook, and D. Mitchell, "Effect of steel Fibers on the Performance of Ultrahigh-Strength Concrete Columns", *Journal if Materials in Civil Engineering*, vol. 27, no. 4, 2015.
[10] H. O. Shin, K. H. Min, D. Mitchell, "Confinement of ultra-high-performance fiber reinforced concrete columns", *Composite Structures*, vol. 176, pp. 124-142, 2017.
[11] H. O. Shin, K.H. Min, D. Mitchell, "Uniaxial behavior of circular ultra-high-performance fiber-reinforced concrete columns confined by spiral reinforcement", *Construction and Building Materials*, vol. 168, pp. 379-393, 2018.
[12] M. M. Hosinieh, H. Aoude, W. D. Cook, and D. Mitchell, "Behavior of ultra-high-performance fiber reinforced concrete columns under pure axial loading", *Engineering Structures*, vol. 99, pp. 388-401, 2015.
[13] G. Steven, and M. Empelmann, "UHPFRC-Columns with high-strength longitudinal reinforcement (in German)", *Concr Reinf Concr*, vol. 109, no. 5, pp. 344-54, 2014.
[14] C. C. Hung, F. Y. Hu, and C. H. Yen, "Behavior of slender UHPC columns under eccentric loading", *Engineering Structures*, vol. 174, pp. 701-711, 2018.
[15] K. Wille, A. E. Naaman, and S. EI-Tawil, "Properties of strain hardeningultra high performance fiber reinforced concrete (UHP-FRC) under direct tensile loading," *Cement and Concrete Composites*, vol. 48, pp. 53–66, 2014.
[16] S. J. Foster, M. M. Attard, "Strength and Ductility of Fiber-Reinforced High-Strength concrete columns," *Journal of Structural Engineering*, vol. 127, no. 1, pp. 28-34, 2001.